Hydrogen-Bond Reinforced Vanadia Nanofiber Paper of High Stiffness

Zaklina Burghard, Andreas Leineweber, Peter A. van Aken, Thomas Dufaux, Marko Burghard, and Joachim Bill*

Paper-like materials have attracted great interest for a wide range of applications, such as protective coatings, adhesive layers, or rolling-up electrodes in batteries or super-capacitors.[1] There has been significant recent progress in enhancing the mechanical properties of papers or foils via the implementation of novel types of inorganic nanoplatelets. The synthesis of papers from ceramics, however, still poses a major challenge due to their high brittleness, which has hampered their widespread technological application. One versatile approach involves pre-ceramic papers as precursors of multilayer ceramic products.[2] More recently, strong attention has been directed toward mimicking the structural design of biomaterials which combine layers of nanosized inorganic tiles of high aspect ratio with a small volume fraction of biopolymer providing sacrificial bonds.[3,4] Examples of ceramic-based papers realized in this manner are foils composed of vermiculite,[5] clay[6,7] or alumina[8] platelets, as well as paper-like films comprising carbon nanostructures like carbon nanotubes[9–11] or graphene oxide.[12–14] Among these, graphene oxide-based papers have recently attracted strong attention due to their remarkable mechanical properties that can be tuned by altering the density of hydrogen bonds between the individual sheets.[15]

Here, we exploit the unique structural properties and self-assembly capability of vanadia (V_2O_5) nanofibers to obtain a paper-like material whose architecture resembles that of structural biomaterials in an unprecedented manner. As distinguished from most other transition metal oxides, vanadium pentoxide has the remarkable property that it can be obtained in the form of crystalline fibers with ultrahigh aspect ratio via a polycondensation process in aqueous solution.[16] The average length of the fibers is adjustable between ≈100 nm and several tens of micrometers by controlling the composition and age of the solution.[17] The ribbon-shaped fibers[16–20] with a rectangular cross-section of ≈1.5 nm × 10 nm are composed of a bilayer of corrugated single sheets[16,19] made of square VO_5 pyramidal units with water molecules residing in between (**Figure 1**a). Due to dissociation of -OH groups at their edge planes, the fibers bear a negative charge.[16] In addition, the basal planes of the fibers bear oxo groups and water molecules, the latter of which are partaking in coordination bonds (Figure 1b). Their highly anisotropic structure and versatile surface chemistry renders V_2O_5 nanofibers into close-to-ideal components of paper-like materials. By contrast, carbon nanotubes and graphene both require functionalization to render them soluble and ensure sufficiently strong interactions between them. At the same time, as-prepared vanadia nanofibers are electrically conductive[20] without the need for chemical conversion like in case of graphene oxide.[21] The multifunctional character of V_2O_5 is complemented by its rich redox chemistry, thus opening a wide variety of applications in catalysis, electrochromic devices, batteries, as well as sensors and actuators.[22–24] Thus far, major attention has been directed to so-called xerogels obtainable through simple drying of V_2O_5 aqueous sols,[25,26] as well as films prepared by vacuum filtering,[27] both of which consist of a loose network of entangled fibers.[19] From such films, actuators have been obtained that operate at lower voltage than conventional ferroelectric and electrostrictive materials.[27] However, these devices exhibit only a slow response due to the low mobility of the intercalated cations, a drawback which limits also other electrochemical applications. In order to increase the operation speed, a suitable method to align the fibers would be highly desirable.[23]

The V_2O_5 fiber sols used in the present study were prepared from ammonium metavanadate, adapting a previously reported procedure.[16] Slow drying of such sols on a substrate yielded homogeneous coatings that can be easily floated-off to yield free-standing, paper-like films (Figure S1 in the Supporting Information). The size and shape of the papers can be tailored by the substrate dimensions, while their thickness ranges between 0.5 and 2.5 μm depending on the sol volume used. Drying of the as-prepared films under controlled humidity yields an optically transparent paper of dark orange color (Figure 1c). Atom force microscopy (AFM) shows that the nanofibers are densely packed and aligned over many μm within the substrate plane (Figure 1d). Moreover, the vanadia paper exhibits an extraordinary mechanical flexibility (i.e., it can be easily bent into harmonica-like three-dimensional structures, or rolled-up into

Dr. Z. Burghard, Prof. J. Bill
Institute for Materials Science
Chair for Chemical Materials Synthesis
University of Stuttgart
Heisenbergstrasse 3, D-70569 Stuttgart, Germany
E-mail: zaklina.burghard@imw.uni-stuttgart.de
Dr. A. Leineweber
Max Planck Institute for Intelligent Systems
Heisenbergstrasse 3, D-70569 Stuttgart, Germany
Prof. P. A. van Aken
Stuttgart Center for Electron Microscopy
Max Planck Institute for Intelligent Systems
Heisenbergstrasse 3, D-70569 Stuttgart, Germany
Dr. T. Dufaux, Dr. M. Burghard
Max Planck Institute for Solid State Research
Heisenbergstrasse 1, D-70569 Stuttgart, Germany

DOI: 10.1002/adma.201300135

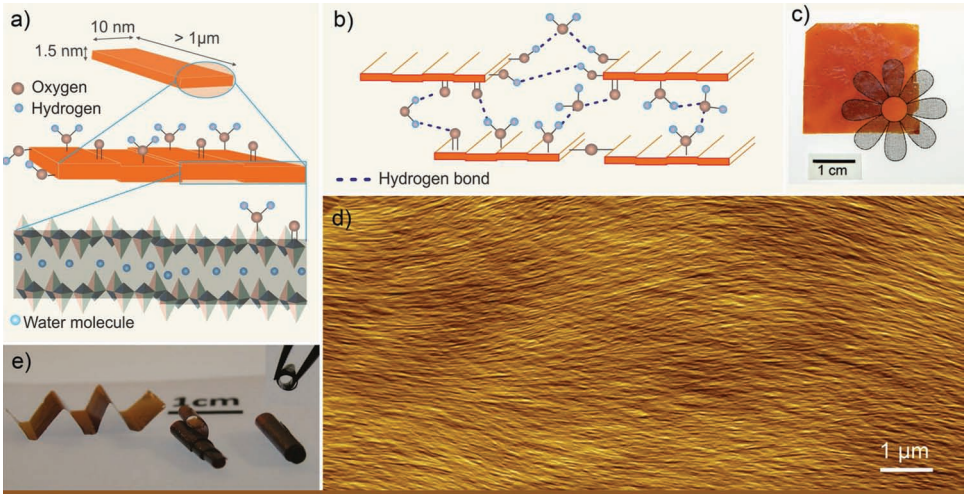

Figure 1. Architecture and mechanical flexibility of the vanadia paper. a) Structure and dimensions of an individual nanofiber. Each fiber is composed of two V_2O_5 layers with a water layer in-between. b) Schematic depiction of the hydrogen-bond network between the V_2O_5 nanofibers. Lateral hydrogen bonds can be formed between the hydroxyl groups at the fiber edges, while in vertical direction both the hydroxyl- and oxo-groups on the fiber surface are involved in hydrogen bonding. Upon annealing, covalent V–O–V bridges can be created between neighboring nanofibers. c) Digital image of a ≈2 µm-thick vanadia paper, demonstrating the optical transparent behavior. d) AFM image of the film surface revealing nanofibers that are well-aligned over many micrometers. e) The high mechanical flexibility of the paper is highlighted by folding into a harmonica-like structure, and rolling-up into a cylinder with a diameter of 1 mm and a length of 30 mm.

spiral-like cylinders or narrow tubes with diameters as small as 1 mm (Figure 1e)).

Inspection of fracture surfaces of the vanadia papers by scanning electron microscopy (SEM) reveals the presence of lamellae stacked on top of each other (**Figure 2**a). The SEM images in particular of the as-prepared vanadia paper furthermore display pulled-out fibers within sheet-like ensembles, indicating a sizable lateral interaction between the fibers. Higher magnification AFM images of the vanadia paper surface display approximately 20 nm wide features, comparable to the width of two nanofibers (Supporting Information, Figure S2), whose narrow endings are closely connected (Figure 2b). In addition to such lateral assembly, transmission electron microscopy (TEM) images of cross-sectional vanadia paper samples, cut parallel to the long fiber axis, reveal single-crystalline fibers stacked in vertical direction (Figure 2c). In order to determine the degree of vertical ordering, we have studied the papers by X-ray diffraction (XRD) (Figure 2d). The observed (001) reflection signifies a layer-to-layer distance (*d*-spacing) of 1.08 nm, slightly smaller than the value of 1.15 nm reported for the hydrated layer phase $V_2O_5 \cdot nH_2O$ (with $n = 1.8$) wherein a one-molecule-thick water layer resides between the vanadia sheets.[16] The mean size of the vertical fiber stacks was calculated using the Scherrer equation to be 5.7 nm, corresponding to a stack of about 4 vanadia fibers. From the AFM and XRD analysis, it follows that the papers are composed of ≈20 nm wide and ≈6 nm thick slabs comprised of nanofibers. This slab width is in good agreement with conclusions drawn from XRD studies of vanadia xerogels.[19] The slab formation can be attributed to a lateral connection of the fibers via oxygen bridges (V–O–V),[19] in conjunction with hydrogen bonds formed between the water molecules on the fiber basal planes (Figure 2e). Assembly of the slabs in lateral direction then leads to formation of the lamellae visible in the SEM images (cf. Figure 2a). The preferred fiber alignment direction varies from lamella to lamella, confirming the flexible connectivity of the hierarchical hydrogen bond network between the fibers. A high flexibility of the paper is manifested in the possibility to imprint its surface with a regular pattern of indents or protrusions (Figure 2f), with achievable feature sizes below 1 µm. In addition, even under strong bending the layer structure is fully preserved without breaking of the fibers (Figure 2g), highlighting the extraordinary elasticity of the vanadia paper and its constituent fibers.

As a consequence of the hydrogen bond network connecting the nanofibers, the mechanical properties of the vanadia paper are expected to be sensitive to water content. To explore the influence of water, we subjected samples dried at 40 °C to annealing at either 100 or 150 °C for 2 h. Such soft annealing is important to preserve the basic structure of the fibers.[16] According to thermogravimetric analysis (TGA), the drying results in a total mass loss of ≈7%, while the subsequent annealing at 100 or 150 °C causes a loss of ≈2.5 or ≈4.5 wt%, respectively (Supporting Information, Figure S3). That the fibers structure indeed remains intact could be confirmed by XRD analysis of the samples. The XRD peak position shift to larger angles observed upon drying/annealing implies a decrease of the interplanar spacing (from 1.08 nm to 1.04 nm), indicating some loss of water from inside the fibers (Supporting Information, Figure S4). Thus, mainly the water weakly adsorbed between the V_2O_5 nanofibers is removed.[16] It should be emphasized that without prior drying, annealing resulted in crack formation and pronounced crumpling of the vanadia paper. A similar beneficial effect of drying has been reported for titania-based nanocomposites.[28,29] Obviously, slow water removal is pivotal to ensure sufficient mobility of the fibers such that they can closely pack together, most likely through the structure-directing capability of the hydrogen bonded water between the V_2O_5 nanofibers (cf. Figure 1b). This smooth assembly process is a major feature distinguishing the present vanadia paper from the less ordered vanadia nanofiber xerogels.

The behavior of the vanadia paper under tensile stress is documented by the stress (σ)–strain (ε) curves in **Figure 3**a–d. All the curves feature two or three distinct regimes, and a weak washboard pattern discernible as a sequence of peaks in the corresponding derivative ($\delta\sigma/\delta\varepsilon$) curves (Figure 3e), comparable to the mechanical response of papers made of graphene oxide,[12–14] carbon nanotubes,[9,10] or clay[6] platelets. However,

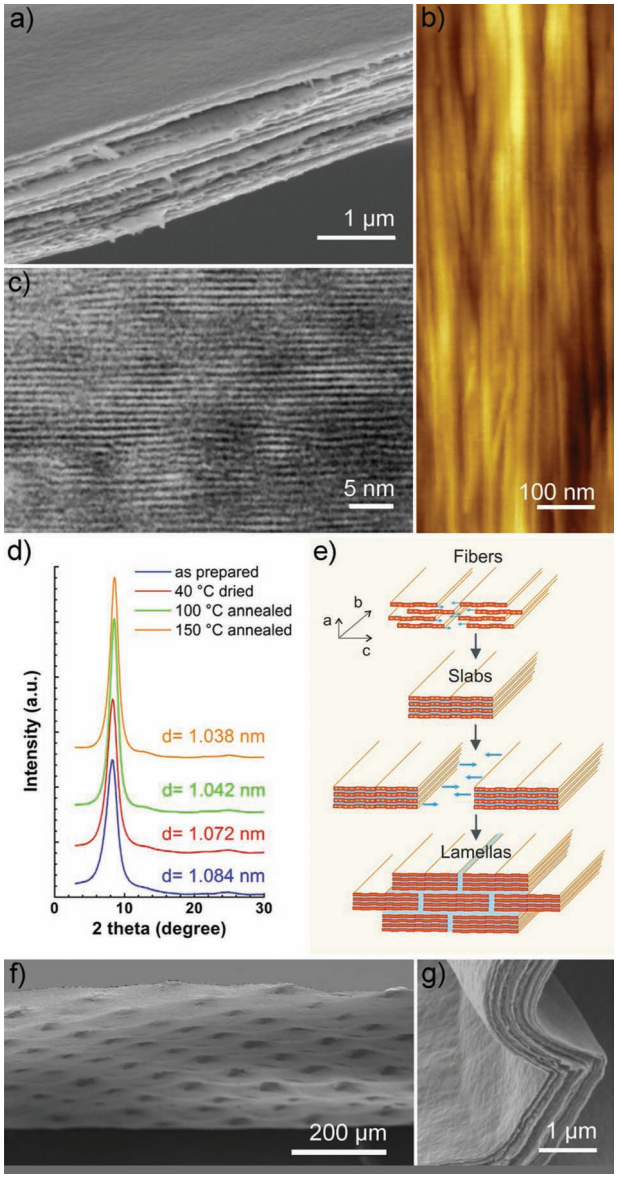

Figure 2. Morphology and microstructure of the vanadia paper. a) SEM micrograph of the fracture surface of a 2.5 µm-thick as-prepared vanadia paper. b) AFM image of the film surface revealing the presence of ≈20 nm wide slabs composed of at least two nanofibers. c) HRTEM image of a cross-section (length fiber axis) of an as-prepared sample. d) X-ray diffraction patterns acquired from vanadia paper subjected to different thermal treatments, with the measured interplanar spacings indicated. e) Schematic representation of the formation of slabs and their assembly into a brick-and-mortar like arrangement wherein oxide fibers as the hard component are surrounded by water as the soft component (*a*, *b*, *c*: height, length, width fiber axis, respectively). f) SEM image of a relief structure on the surface of a vanadia paper, representing a replicate of the underlying sieve used for drying. g) SEM image of a vanadia paper that is strongly bent and kinked without losing its structural integrity.

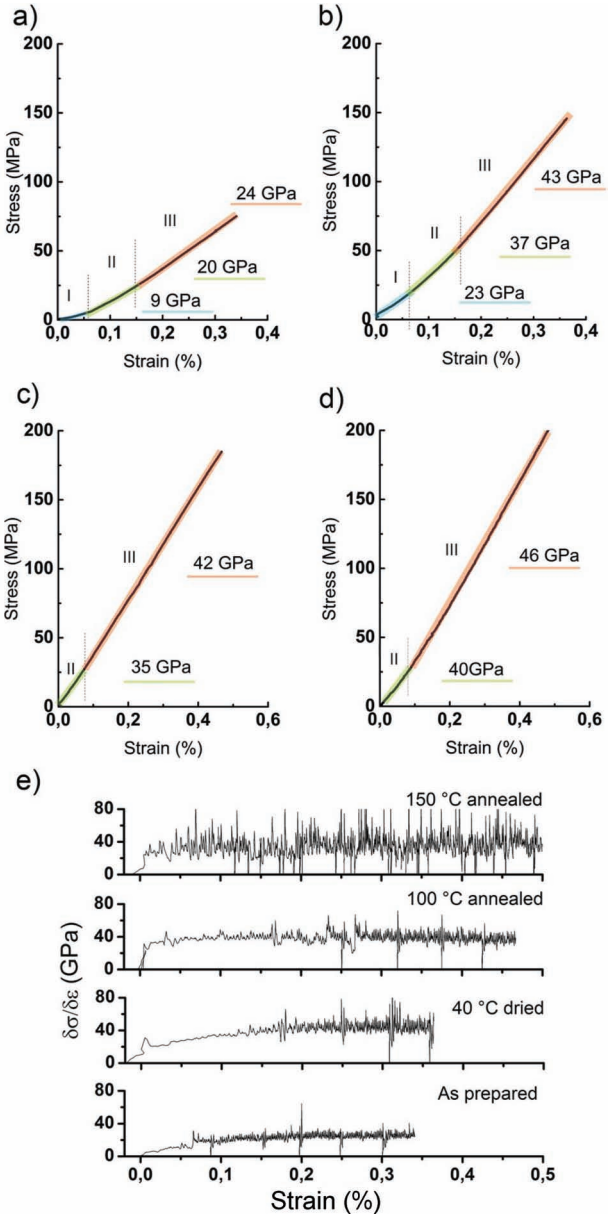

Figure 3. Tensile behavior of the vanadia paper in dependence of water content. (a–d). Stress–strain curves obtained from a sample stored for 48 h under ambient conditions (a), after drying at 40 °C for 16 h under controlled humidity (b), and after subsequent annealing at either 100 °C (c) or 150 °C (d) for 2 h. e) Derivatives of the stress–strain curves in panels a–d.

in contrast to the latter, no plateau is reached under highest strain, which is characteristic of ceramic materials that do not undergo plastic deformation. Correspondingly, the vanadia paper exhibits a much higher stiffness of 46 GPa after annealing at 150 °C. The as-prepared and dried vanadia paper samples display an initial loading regime (I), followed by a straightening (II), and finally a linear elastic regime (III). The loading regime (I) displays a gradual increase of modulus, indicative of easy deformation associated with the elimination of bulk structural irregularities like the waviness introduced during sample drying (Supporting Information, Figure S5). This signifies the soft character of the papers before annealing, which derives from the sizable amount of water weakly bonded between the vanadia fiber slabs. Upon water removal, the

loading regime, as expected, becomes less pronounced for the dried vanadia paper, and vanishes completely after annealing. In the straightening regime (II), "mechanical annealing" occurs via lateral rearrangement of the fibers, with the resulting reinforcement leading to an abrupt increase in the derivative curve. Finally, within the linear elastic regime (III) disruption of the hydrogen bonds between the slabs and deformation of the covalent oxygen bridges between the fibers occurs, as reflected by the more pronounced washboard pattern. After annealing, the ultimate strain reaches ≈0.45%, comparable to values reported for graphene oxide-based papers.[12,14]

Water removal was found to increase also the vanadia papers' toughness and tensile strength (see Supporting Information, Table S1). Upon annealing, the toughness (i.e., work of fracture) increases to ≈480 kJ m^{-3}, as compared to ≈75 and ≈210 kJ m^{-3} for the as-prepared and dried samples, respectively. The toughness after annealing is superior to the best values documented for graphene oxide papers of similar thickness (≈320 kJ m^{-3}).[12] Likewise, the tensile strength increases substantially from ≈76 MPa for the as-prepared samples to ≈132 MPa after drying, and further to ≈200 MPa after annealing. Based upon discussion of the stress/strain regimes, we attribute the limited toughness and tensile strength of the non-annealed vanadia paper sample to the weak connection of the slabs due to the relatively high amount of water in between them. AFM investigation suggests that this water exists as a sheath around the nanofiber slabs in the as-prepared vanadia papers (**Figure 4**a), while after drying they appear thinner and straightened (Figure 4b). This change may result from a smooth interlocking of the corrugated basal planes of the fibers upon slow water removal (compare Figure 1a and 2e), which in turn can explain the absence of fiber pullout in the fracture surface (Figure 4c). The interlocking is expected to increase the hydrogen-bond density between –OH groups on the fibers, thereby promoting effective energy dissipation and stress distribution between the fibers through stretching of the hydrogen bonds around the fibers, akin to intermediate-strength bonds in tightly folded macromolecules in biomaterials.[30] The further enhancement of mechanical performance upon subsequent annealing is attributable to the formation of covalent V–O–V bonds between the slabs in vertical and lateral direction. Such bridge formation has been documented for vanadia xerogels above 200 °C,[16] however, in our vanadia paper it may more readily occur due to the closer and ordered arrangement of the fibers. The oxygen bridges are also expected to impede the crack propagation, thus accounting for the observed toughness increase. Similar reinforcement has been attained using divalent cations to cross-link graphene oxide sheets.[14] It is furthermore noteworthy that the Young's modulus remains almost unaffected by the annealing (40–45 GPa), suggesting that oxygen bridge formation restricts structural reorganization via sliding of the fibers with respect to each other.

In Figure 4d, the maximum achieved tensile strength and Young's modulus of the investigated V_2O_5 nanofiber papers is compared to the best literature values reported for single component paper-like materials (without further reinforcement by bifunctional linkers or metal ions), including carbon nanostructure-based papers,[10,12,14] vanadia sheets[27] and nacre.[31] The excellent mechanical performance of the present paper,

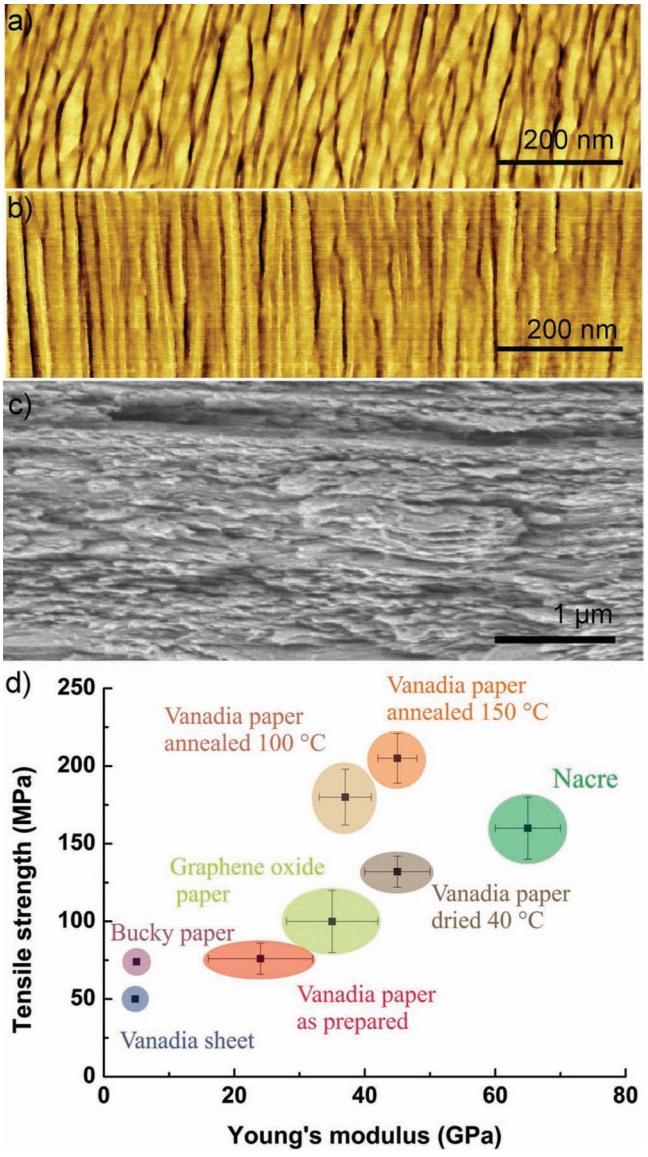

Figure 4. Assessment of mechanical performance. a,b) AFM image of an as-prepared vanadia paper sample (a), and a sample after drying at 40 °C and subsequent annealing at 100 °C (b). c) SEM image of the fracture surface of a vanadia paper annealed for 2 h at 150 °C. d) Comparison of tensile strength and Young's modulus of our vanadia paper subjected to different thermal treatments with values reported for other major types of paper-like materials.

documented by values comparable or superior to those of the other materials, can be attributed to the alternating layer structure of the vanadia paper, comprising a stiff inorganic oxide component combined with "flexible" layers of water molecules in between (Figure 2e), strongly resembling the brick-and-mortar architecture of structural biomaterials like nacre[31,32] which introduces a similar toughening mechanism.[30–33] Indeed, the vertically stacked nanofibers may assume a similar function like the micrometer-sized mineral platelets in nacre (Supporting Information, Figure S7), while the water

sheath around the fibers acts as soft, deformable component of the paper. Major contributing factors are the presence of single-crystalline oxide fibers with high aspect ratio and strong internal covalent bonds, the fibers' interlocking capability (under the condition of optimized water content), as well as the hydrogen bond network between the fibers. The tenfold higher stiffness and 4 times larger strength in comparison with filtration-derived vanadia nanofiber sheets[27] highlight the better order and alignment of the fibers in our vanadia paper. Compared to nacre, the annealed vanadia paper reaches higher strength, although its stiffness is lower (≈45 GPa vs. ≈70 GPa for nacre). The latter difference likely originates from the smaller volume ratio between the hard and soft component in the vanadia paper. Overall, the dense packing of the fibers achieved by self-assembly, combined with their hierarchical organization (fibers–slabs–lamellas), yield an excellent combination of stiffness and toughness of the vanadia papers.

Besides the mechanical properties, the ordered layer structure of our vanadia papers is also manifested in their electrical conductivity characteristics (see Supporting Information, Table S2). We have measured the in-plane and out-of-plane conductivity of the papers under ambient conditions. After drying at room temperature, the paper exhibits an in-plane conductivity of 1.8 S/cm, slightly higher than the values ranging from 0.5–1 S/cm reported for the less ordered vanadia xerogels.[16] In agreement with the above described increase in the structural order of the vanadia paper after annealing at 40 °C under controlled humidity, the conductivity shows an increase by more than 10% after such treatment. Annealing at either 100 or 150 °C decreases the conductivity by approximately 2%. That such decrease occurs already at 100 °C might result from a reduced ionic contribution to the total conductivity, as the former is known to decrease with decreasing water content in V_2O_5 nanofiber xerogels.[16] Moreover, the absence of a significant further reduction of conductivity after annealing at 150 °C indicates a still efficient contact between the current-carrying crystalline regions in the layers. It is furthermore noteworthy that the vanadia paper exhibits a pronounced conductivity anisotropy between the in-plane and out-of-plane directions. In fact, for all investigated annealing conditions the out-of-plane conductivity falls roughly three orders of magnitude below the in-plane value, consistent with the well-ordered layer structure of the paper.

While the water layer within and surrounding the vanadia nanofibers imparts the excellent mechanical flexibility to our vanadia paper, it should be possible to further improve its mechanical properties by the incorporation of organic polyelectrolytes,[9,29,34] metal ions[14] or organic bifunctional linkers.[11,34,35] Furthermore, the well-established intercalation capability and rich redox chemistry of V_2O_5 render the vanadia paper prospective for a wide range of applications in the fields of stretchable electronics and energy storage, in particular as flexible electrodes in chemical sensors, actuators, electrochromic devices, batteries or supercapacitors. A good performance of such electrodes is expected from the excellent toughness of the paper, which could reduce crack formation due to volume changes associated with ion intercalation.

Experimental Section

The V_2O_5 nanofiber colloidal solution was prepared from ammonium meta-vanadate (1 g, Aldrich) and acidic ion-exchange resin (10 g, Dowex 50WX8, Alfa Aesar) in 200 ml of deionized water (200 ml). This mixture was heated under stirring to 80 °C for 10 min, and then slowly cooled to room temperature. The sol was aged for 2 weeks under ambient conditions, which yielded fibers with an average length of 5 µm. Details about the sample preparation are provided in the Supporting Information. Controlled drying and annealing of the vanadia papers was carried out in a climate test chamber VC 7018 (Vötsch).

The vanadia paper's micro/nanostructure was investigated by light microscopy (Axiophot, Zeiss) and scanning electron microscopy (Leo 1530 VP Gemini, Zeiss). The surface topography of the films was determined by atomic force microscopy (Dimension Icon, Bruker). High resolution transmission electron microscopy investigations were performed on thinned samples prepared by focused-ion-beam milling using a JEOL 4000FX microscope.

The tensile strength of the vanadia papers was determined by nanotensile testing (Nano Bionix, MTS Nano Instruments) of 0.5–1 mm × 10 mm samples with a thickness of ≈2.5 µm (as detected by electron microscopy of the paper fracture surface), using the controlled force mode with a strain rate of 1×10^{-5} s^{-1} and a load resolution of 50 nN. For this purpose, the samples were glued on a holder made of board paper (see Supporting Information). Thermogravimetric analysis was performed with a Netzsch STA 409 instrument within the temperature range of 0–350 °C, applying a slow heating rate of 1 °C min^{-1}. X-ray diffraction experiments were carried out at room temperature using Cu K_α radiation (Bruker D8-Discover instrument operated at 40 keV and a cathode current of 40 mA, working in parallel-beam geometry). For determination of the crystallite size according to the Scherrer equation, previously determined instrumental broadening was considered before attributing the additional line broadening purely to crystallite-size broadening. Electrical conductivity measurements were done under ambient conditions using manually attached silver paste electrodes in four-terminal configuration, with the 5 mm wide and 30 mm long samples fixed in a special holder (see Supporting Information).

Supporting Information

Supporting Information is available from the Wiley Online Library or from the author.

Acknowledgements

The authors are grateful to R. Mager for sample preparation for the mechanical and electrical measurements and performing tensile tests, M. Huang and A. Knöller for sample fabrication, B. Heiland for specimen preparation by ion-beam thinning, T. Wörner for technical support, P. Kopold for HRTEM investigations, B. Fenk and C. Greiner for SEM investigations, G. Maier for XRD investigations, and T. Lehman for TGA measurements. The financial support from the DFG (BI 469/17-1) is greatly acknowledged.

Received: January 10, 2013
Published online: March 7, 2013

[1] M. J. Pitkethly, *Mater. Today* **2004**, *7*, 20.
[2] N. Travitzky, H. Windsheimer, T. Fey, P. Greil, *J. Am. Ceram. Soc.* **2008**, *91*, 3477.
[3] K. Liu, L. Jiang, *Nano Today* **2011**, *6*, 155.
[4] J. Wang, Q. Cheng, Z. Tang, *Chem. Soc. Rev.* **2012**, *41*, 1111.

[5] D. G. H. Ballard, G. R. Rideal, *J. Mater. Sci.* **1983**, *18*, 545.
[6] Z. Tang, N. A. Kotov, S. Magonov, B. Ozturk, *Nat. Mater.* **2003**, *2*, 413.
[7] A. Walther, I. Bjurhager, JM. Malho, J. Ruokolainen, L. Berglund, O. Ikkala, *Angew. Chem. Int. Ed.* **2010**, *49*, 6448.
[8] L. J. Bonderer, A. R. Studart, L. J. Gauckler, *Science* **2008**, *319*, 1069.
[9] A. A. Memedov, N. A. Kotov, M. Prato, D. M. Guldi, J. P. Wicksted, A. Hirsch, *Nat. Mater.* **2002**, *1*, 190.
[10] X. Y. Zhang, T. V. Sreekumar, T. Liu, S. Kumar, *J. Phys. Chem. B* **2004**, *108*, 16435.
[11] Q. Cheng, M. Li, L. Jiang, Z. Tang, *Adv. Mater.* **2012**, *24*, 1838.
[12] D. A. Dikin, S. Stankovich, E. J. Zimney, D. R. Piner, G. H. B. Dommett, G. Evmenko, S. T. Nguyen, R. S. Ruoff, *Nature* **2007**, *448*, 457.
[13] Y. Q. Li, T. Yu, T. Y. Yang, L. X. Zheng, K. Liao, *Adv. Mater.* **2012**, *24*, 3426.
[14] S. Park, K. Lee, G. Bozoklu, W. Cai, S. T. Nguyen, R. S. Ruoff, *ACS Nano* **2008**, *2*, 572.
[15] N. V. Medheker, A. Ramasubramaniam, R. S. Ruoff, V. B. Shenoy, *ACS Nano* **2010**, *4*, 2300.
[16] J. Livage, *Chem. Mater.* **1991**, *3*, 578.
[17] J. Livage, *J. Coord. Chem. Rev.* **1998**, *999*, 178–180.
[18] T. Yao, Y. Oka, N. Yamamoto, *Mater. Res. Bull.* **1992**, *27*, 669.
[19] V. Petkov, P. N. Trikalitis, E. S. Bozin, S. J. L.Billinge, T. Vogt, M. G. Kanatzidis, *J. Am. Chem. Soc.* **2002**, *124*, 10157.
[20] J. Muster, G. T. Kim, V. Krstic, G. J. Park, Y. W. Park, S. Roth, M. Burghard, *Adv. Mater.* **2000**, *12*, 420.
[21] C. Gomez-Navarro, R. T. Weitz, A. M. Bittner, M. Scolari, A. Mews, M. Burghard, K. Kern, *Nano Lett.* **2007**, *7*, 3499.
[22] I. Raible, M. Burghard, U. Schlecht, A. Yasuda, T. Vossmeyer, *Sens. Actuators B* **2005**, *106*, 730.
[23] J. Livage, *Nat. Mater.* **2003**, *2*, 297.
[24] L. Mai, X. Xu, L. Xu, C. Han, Y. Luo, *J. Mater. Res.* **2011**, *26*, 2175.
[25] G. S. Zakharova, V. L. Volkov, *Russ. Chem. Rev.* **2003**, *72*, 311.
[26] P. C. R. Davidson, *Chimie* **2010**, *13*, 142.
[27] G. Gu, M. Schmid, P. W. Chiu, A. Minett, J. Fraysse, G. T. Kim, S. Roth, M. Kozlov, E. Munoz, R. H. Baughman, *Nat. Mater.* **2003**, *2*, 316.
[28] A. Razgon, C. N. Sukenik, *J. Mater. Res.* **2005**, *20*, 2544.
[29] Z. Burghard, L. Zini, V. Srot, P. Bellina, P. A. van Aken, J. Bill, *Nano Lett.* **2009**, *9*, 4103.
[30] B. L. Smith, T. E. Schäffer, M. Viani, J. B. Thompson, N. A. Frederick, J. Kindt, A. Belcher, G. D. Stucky, D. E. Morse, K. P. Hansma, *Nature* **1999**, *399*, 761.
[31] M. Sarikya, *Microsc. Res. Techn.* **1994**, *27*, 360.
[32] M. A. Meyers, P. Y. Chen, A. Y. M. Lin, Y. Seki, *Prog. Mater. Sci.* **2008**, *53*, 1.
[33] P. Fratzl, H. S. Gupta, F. D. Fischer, O. Kolednik, *Adv. Mater.* **2007**, *19*, 2657.
[34] P. Podsiadlo, A. K. Kaushik, E. M. Arruda, A. M. Waas, B. S. Shim, J. D. Xu, H. Nandivada, B. G. Pumplin, J. L. Ramamoorthy, N. A. Kotov, *Science* **2007**, *318*, 80.
[35] G. Gannon, C. O'Dwyer, J. A. Larsson, D. Thompson, *J. Phys. Chem. B* **2011**, *115*, 14518.